IEEE Access
Multidisciplinary | Rapid Review | Open Access Journal

Received December 16, 2018, accepted December 26, 2018, date of publication January 3, 2019, date of current version February 22, 2019.

Digital Object Identifier 10.1109/ACCESS.2018.2890561

Joint Weighted Tensor Schatten p-Norm and Tensor l_p-Norm Minimization for Image Denoising

XIAOQIN ZHANG, (Member, IEEE), JINGJING ZHENG, YUFANG YAN, LI ZHAO, AND RUNHUA JIANG

Department of Computer Science, Wenzhou University, Wenzhou 325035, China

Corresponding author: Li Zhao (lizhao@wzu.edu.cn)

This work was supported in part by the National Natural Science Foundation of China under Grant 61772374, Grant 61472285, and Grant 61503263, in part by the Zhejiang Provincial Natural Science Foundation under Grant LY17F030004, Grant LR17F030001, Grant LQ18F030010, and Grant LQ19F020005, in part by the Project of Science and Technology Plans of Zhejiang Province under Grant 2015C31168, and in part by the Project of Science and Technology Plans of Wenzhou City under Grant C20170008, Grant G20160002, Grant G20170010, Grant G20150017, and Grant ZG2017016.

ABSTRACT In the traditional non-local similar patch-based denoising algorithms, the image patches are firstly flatted into a vector. The structure information within the image patches is ignored; however, the spatial layout information can be used for improving the denoising performance. To solve this problem, this paper treats the image patches as matrices and proposes a low-rank tensor recovery model for image denoising, and thus it makes full use of spatial information within the image. Meanwhile, the proposed model can realize joint weighted tensor Schatten p-norm and tensor l_p-norm minimization, which has two advantages: 1) it can deal with zero mean Gaussian noise, impulse noise, and any other noise that can be approximated by mixing these two kinds of noise and 2) the employed norms require relatively weak incoherence conditions than l_1 norm and nuclear norm, and thus they are more robust against outliers and noise. The experimental results show that the proposed algorithm outperforms other state-of-the-art denoising algorithms in both visual perception quality and quantitative measures.

INDEX TERMS Image denoising, low-rank tensor recovery, tensor Schatten p-norm.

I. INTRODUCTION

Image denoising is a basic problem in the field of image processing, and a lot of related algorithms have been proposed in the past few decades. The existing image denoising methods are mainly divided into two types: local methods and nonlocal methods. Local methods [1], [2] usually use certain filter to do convolution operation for the whole image, which ignores the global structure information of image and makes the denoised image lose detail. To deal with this issue, a pioneering work, the Nonlocal Means (NLM) algorithm, has been proposed that applies the non-local strategy to image denoising and makes full use of self-similarity of images to remove noise. Because of good performance of NLM, a large number of image denoising methods based on nonlocal method appeared [3]–[8].

Besides, low rank matrix approximation (LRMA) appeals to significant research interest, and it devotes to recovering the underlying low rank matrix from its degraded version. Low rank matrix approximation can be divided into two categories: the low rank matrix factorization (LRMF) methods [10], [11] and the rank minimization methods [12]–[16]. In this paper, we focus on the latter. The rank of a matrix $X \in R^{m\times n}$ is defined as the number of its nonzero singular values. Since the original rank minimization problem is NP-hard, Candes and Recht [17] and Cai *et al.* [18] put forward the nuclear norm minimization (NNM) problem to approximate the original problem, and have proven the equivalence of two problems in some cases. Since NNM is a convex problem, it can be solved easily.

The singular values have explicit physical sense, and thus should be treated in different ways. However, the nuclear norm minimization regularizes each singular value equally which greatly restricts its capability and exibility in image denoising. To address this issue, Dong *et al.* [3] propose a spatially adaptive iterative singular-value thresholding image denoising method (SAIST) which utilizes variance estimation

for the denoised image and deals with different singular values in different ways. Later, Gu *et al.* [4] propose an image denoising algorithm via weighted nuclear norm minimization, in which the larger singular values have smaller weight to ensure that the less they should be shrunk. Hosono *et al.* [9] give a color image denoising method via Weighted Tensor Nuclear Norm Minimization (WTNN) which stacks the nonlocal similar patches into a matrix in each color channel and processes all color channels jointly. Since the solution of NNM can seriously deviate from the original solution of rank minimization problem in practice [19], the weighted Schatten p-norm minimization method [21] has been proposed to get a more accurate recovery of signal [20].

Although the above image denoising algorithms have achieved great success, they have two major limitations: (1) All the above denoising algorithms are proposed to deal with zero mean Gaussian noise and thus their models are very sensitive to outliers, and large errors may arise even for a single pixel. In fact, except for the rather academic excercise ''add noise and then remove it'', this assumption cannot be satisfied in most real-world image denoising applications. (2) In contrast to the local methods, nonlocal image denoising methods completely ignore the spatial layout information within the image which contributes to promote the denoising performance.

In order to solve the mentioned problems, we propose a joint weighted tensor schatten p-norm and tensor l_p-norm minimization (WTSTP) model for image denoising. The features of the proposed algorithm are two-fold: (1) the proposed algorithm treats the image patches as tensor (or matrix for grayscale image) to preserve the structure information and the relation of different channels within the image patches. (2) WTSTP guarantees a more accurate low-rank recovery and thus is robust against noise and outliers.

The rest of this paper is organized as follows. We bring up WTSTP from traditional low-rank recovery model, and analyze its optimization scheme in Section II. In Section III, we give image denoising algorithm based on WTSTP to remove noise in grayscale image and color image. The experimental results are presented in Section IV, and Section V concludes the paper.

II. JOINT WEIGHTED TENSOR SCHATTEN *P*-NORM AND TENSOR L_P-NORM MINIMIZATION

A. TRADITIONAL LOW-RANK RECOVERY MODEL

Given an observed matrix $Y \in R^{m\times n}$, the aim of the original rank minimization is to find a low rank matrix $\hat{X}$ which satisfies the following objective function:

$$\hat{X} = \arg\min_{X} \frac{1}{2}\|Y - X\|_F^2 + \alpha \mathrm{rank}(X), \tag{1}$$

where $X \in R^{m\times n}$, $\mathrm{rank}(X)$ is defined as the number of its nonzero singular values, and α is a tradeoff parameter to balance the data fidelity and regularization.

As stated in Section I, the mixed noise of zero mean Gaussian noise and impulse noise is more reasonable and commonly encountered in the real image denoising applications. While the above model is unable to handle the complicated situation, therefore the following model is considered [12]:

$$(\hat{L}, \hat{E}) = \arg\min_{L,E} \frac{1}{2}\|P - L - E\|_F^2 + \alpha \mathrm{rank}(L) + \beta\|E\|_0, \tag{2}$$

where $\|E\|_0$ counts the number of nonzero entries of E, α and β are tradeoff parameters to balance the data fidelity and regularization. In (2), a given matrix $P \in R^{m\times n}$ can be regarded as a noised image matrix, $P-L-E$ and E represent zero mean Gaussian noise and impulse noise respectively.

However, most of the visual data, such as color image and video, have the form of tensor. The traditional image and video processing method prefer to transform the data into 2D matrix for processing. But, as [22] points out, the important structures will be lost when a higher-order tensor is treated as a 2D matrix. Therefore, it is desirable to extend the framework of low-rank matrix recovery to tensor space [22], [23],

$$\min_{\alpha,\varepsilon} \frac{1}{2}\|\mathcal{P} - \mathcal{L} - \mathcal{E}\|_F^2 + \alpha rank(\mathcal{L}) + \beta\|\mathcal{E}\|_0, \tag{3}$$

where $\mathcal{P}$, $\mathcal{E}$ and $\mathcal{L} \in \mathbb{R}^{I_1\times I_2\times\cdots\times I_h}$ are h-order tensors. l_0 norm of tensor $\mathcal{E}$ is defined as $\|\mathcal{E}\|_0 = \|\mathcal{E}_{(i)}\|_0$, where $\mathcal{E}_{(i)}$ is unfolding matrix of tensor $\mathcal{E}$ on the i-th mode. Inspired by the Tuncker decomposition [24], $rank(\mathcal{L})$ is defined as $\Sigma_{i=1}^{h}\lambda_i rank(\mathcal{L}_{(i)})$, where λ_i is a non-negative parameter satisfying $\Sigma_{i=1}^{h}\lambda_i = 1$ and $\mathcal{L}_{(i)}$ is unfolding matrix of tensor $\mathcal{L}$ on the i-th mode.

Because both rank function and the l_0-norm are discontinuous and nonconvex, (3) is hard to solve. Hence, the following model [25] has been put forward,

$$\min_{\alpha,\varepsilon} \frac{1}{2}\|\mathcal{P} - \mathcal{L} - \mathcal{E}\|_F^2 + \alpha\|\mathcal{L}\|_* + \beta\|\mathcal{E}\|_1, \tag{4}$$

where $\|\mathcal{L}\|_* = \Sigma_{i=1}^{h}\lambda_i\|\mathcal{L}_{(i)}\|_*$ and λ_i is a non-negative parameter satisfying $\Sigma_{i=1}^{h}\lambda_i = 1$. References [25] and [26] have shown that the optimal solution of (3) can be perfectly recovered by (4) under certain conditions. Unfortunately, that condition is difficult to satisfy. In the real applications, the solution can be seriously deviated from the original solution of (3). In order to balance the solvability and performance of the model, a joint weighted tensor schatten p-norm and tensor l_p-norm minimization (WTSTP) model is put forward in this paper that is described in the next subsection.

B. THE PROPOSED MODEL

Before introducing WTSTP, the definition of the weighted tensor Schatten p-norm of $\mathcal{L} \in \mathbb{R}^{I_1\times I_2\times\cdots\times I_h}$ and the tensor l_p-norm of $\mathcal{E} \in \mathbb{R}^{I_1\times I_2\times\cdots\times I_h}$ are given as follows:

$$\|\mathcal{L}\|_{\mathbf{w},S_p}^p = \Sigma_{i=1}^{h}\lambda_i\|\mathcal{L}_{(i)}\|_{\mathbf{w}_i,S_p}^p,\ \|\mathcal{E}\|_{p,p}^p = \|\mathcal{E}_{(i)}\|_{p,p}^p \tag{5}$$

where λ_i is a non-negative parameter satisfying $\Sigma_{i=1}^{h}\lambda_i = 1$; $\mathcal{L}_{(i)}$ is unfolding matrix of tensor $\mathcal{L}$ on the i-th mode; $\mathbf{w} = [\mathbf{w}_1^T, \ldots \mathbf{w}_h^T]$, $\mathbf{w}_i$ is the weight vector of each weighted

Schatten p-norm, $1 \le i \le h$ and $h = 3$; $\|\mathcal{L}_{(i)}\|^p_{\mathbf{w}_i,S_p} = \Sigma_{j=1}^{r_{(i)}}(\mathbf{w}_i)_j\sigma_j^p(\mathcal{L}_{(i)})$, where $r_{(i)}$ is the rank of matrix $\mathcal{L}_{(i)}$ and $\sigma_j(\mathcal{L}_{(i)})$ is the j-th singular value of matrix $\mathcal{L}_{(i)}$, $1 \le j \le r_{(i)}$; $\|\mathcal{E}_{(i)}\|^p_{p,p} = \Sigma_{j,k}|e^{(i)}_{jk}|^p$, where $e^{(i)}_{jk}$ is the element of $\mathcal{E}_{(i)}$ in position (j,k). The weighted tensor Schatten p-norm and the tensor l_p-norm (5) are used as the regularizations, and WTSTP is defined as follows:

$$\min_{\alpha,\varepsilon} \frac{1}{2}\|\mathcal{P}-\mathcal{L}-\mathcal{E}\|_F^2 + \alpha\|\mathcal{L}\|^p_{\mathbf{w},S_p} + \beta\|\mathcal{E}\|^p_{p,p} \tag{6}$$

where α, β are two regularization coefficients and $\frac{1}{2}$ is for ease of calculation.

C. OPTIMIZATION ALGORITHM

A series of auxiliary matrices M_i are introduced to replace $\mathcal{L}_{(i)}$ and to remove the correlation of $\mathcal{L}_{(i)}$. Then (6) changes to:

$$\begin{cases} \min_{M_i,\mathcal{L},\mathcal{E}} \frac{1}{2}\|\mathcal{P}-\mathcal{L}-\mathcal{E}\|_F^2 + \alpha\Sigma_{i=1}^h\lambda_i\|M_i\|^p_{\mathbf{w}_i,S_p} \\ \qquad\qquad + \beta\|\mathcal{E}\|^p_{p,p} \\ s.t. \mathcal{L}_{(i)} = M_i, \quad i = 1,2,\ldots h. \end{cases} \tag{7}$$

The Augmented Lagrange Multiplier (ALM) [27] is applied to relax the equality constraints of (7), then the following function is obtained:

$$\begin{aligned} &f_\mu(M_i,\mathcal{E},\mathcal{L},Q_i) \\ &\quad= \frac{1}{2}\|\mathcal{P}-\mathcal{L}-\mathcal{E}\|_F^2 + \alpha\Sigma_{i=1}^h\lambda_i\|M_i\|^p_{\mathbf{w}_i,S_p} + \beta\|\mathcal{E}\|^p_{p,p} \\ &\qquad+ \Sigma_{i=1}^h(\langle Q_i, \mathcal{L}_{(i)}-M_i\rangle + \frac{\mu_i}{2}\|\mathcal{L}_{(i)}-M_i\|_F^2), \end{aligned} \tag{8}$$

where μ_i is a positive scalar, Q_i is Lagrange multiplier matrix and $\langle\cdot,\cdot\rangle$ is the inner product of matrix. Next, alternating direction method (ADM) [27] is used to solve (7):

$$\begin{cases} M_i^{k+1} = \arg\min_{M_i} f_\mu(M_i,\mathcal{E}^k,\mathcal{L}^k,Q_i^k), \quad \forall i=1,2,\ldots,h \\ \mathcal{L}^{k+1} = \arg\min_{\mathcal{L}} f_\mu(M_i^{k+1},\mathcal{E}^k,\mathcal{L},Q^k) \\ \mathcal{E}^{k+1} = \arg\min_{\mathcal{E}} f_\mu(M_i^{k+1},\mathcal{E},\mathcal{L}^{k+1},Q^k) \\ Q_i^{k+1} = Q_i^k + \mu_i(\mathcal{L}_{(i)}^{k+1} - M_i^{k+1}), \quad \forall i=1,2,\ldots,h \end{cases} \tag{9}$$

For term M_i^{k+1}:

$$\begin{aligned} M_i^{k+1} &= \arg\min_{M_i} \lambda_i\|M_i\|^p_{\mathbf{w}_i,S_p} + \langle Q_i^k, \mathcal{L}_{(i)}^k - M_i\rangle + \frac{\mu_i}{2}\|\mathcal{L}_{(i)}^k \\ &\quad - M_i\|_F^2 \\ &= \arg\min_{M_i} \frac{\lambda_i}{\mu_i}\|M_i\|^p_{\mathbf{w}_i,S_p} + \frac{1}{2}\|\mathcal{L}_{(i)}^k + \frac{1}{\mu_i}Q_i^k - M_i\|_F^2 \end{aligned} \tag{10}$$

Ordering $\mathcal{L}_{(i)}^k + \frac{1}{\mu_i}Q_i^k = U\Sigma V^T$, $\Sigma = \mathrm{diag}(\sigma_1,\sigma_2,\ldots\sigma_r)$. According to [28], $\delta_j = GST(\sigma_j, \frac{\lambda_i}{\mu_i}(\mathbf{w}_i)_j, p, J)$ $(j = 1,2,\ldots,r)$ (see Algorithm 1), where J is iteration number of the algorithm, $\Delta = \mathrm{diag}(\delta_1,\delta_2,\ldots,\delta_r)$ and the solution of M_i^{k+1} can be obtained by $M_i^{k+1} = U\Delta V^T$.

Algorithm 1 $x = \mathrm{GST}(y,\lambda,p,J)$ [28]

Input: y, λ, p, J
Output: x
if $|y| \le (2\lambda(1-p))^{\frac{1}{2-p}} + \lambda p(2\lambda(1-p))^{\frac{p-1}{2-p}}$
then
  $x = 0$
else
  $i = 0, x^{(i)} = |y|$
  Iterate on $k = 0, 1, 2, \cdots, J$
  $x^{(i+1)} = |y| - \lambda p(x^{(i)})^{p-1}$
  $k = k + 1$
  $x = \mathrm{sign}(y)x^{(i+1)}$
end

For term $\mathcal{L}^{k+1}$:

$$\begin{aligned} \mathcal{L}^{k+1} &= \arg\min_{\mathcal{L}} \frac{1}{2}\|\mathcal{P}-\mathcal{L}-\mathcal{E}^k\|_F^2 + \Sigma_{i=1}^h(\langle Q_i^k, \mathcal{L}_{(i)} \\ &\quad - M_i^{k+1}\rangle + \frac{\mu_i}{2}\|\mathcal{L}_{(i)} - M_i^{k+1}\|_F^2) \\ &= \arg\min_{\mathcal{L}} \frac{1}{2}\|\mathcal{P}-\mathcal{L}-\mathcal{E}^k\|_F^2 + \Sigma_{i=1}^h\frac{\mu_i}{2}\|\mathcal{L}_{(i)} + \frac{1}{\mu_i}Q_i^k \\ &\quad - M_i^{k+1}\|_F^2 \\ &= v\arg\min_{\mathcal{L}} \frac{1}{2}\|\mathcal{P}-\mathcal{L}-\mathcal{E}^k\|_F^2 + \Sigma_{i=1}^h\frac{\mu_i}{2}\|\mathcal{L} \\ &\quad - \mathrm{refold}_i(M_i^{k+1} - \frac{1}{\mu_i}Q_i^k)\|_F^2, \end{aligned} \tag{11}$$

where $\mathrm{refold}_i(\cdot)$ is the inverse operation of the mode-i unfolding. Next, calculate the partial derivative of objective function of (11) with respect to $\mathcal{L}$, and set it to zero.

$$-\mathcal{P} + \mathcal{L} + \mathcal{E}^k + \Sigma_{i=1}^h\mu_i(\mathcal{L} - \mathrm{refold}_i(M_i^{k+1} - \frac{1}{\mu_i}Q_i^k)) = 0 \tag{12}$$

After rearranging the term with $\mathcal{L}$, the following form is obtained:

$$\mathcal{L} = \frac{\mathcal{P} - \mathcal{E}^k + \Sigma_{i=1}^h\mu_i\mathrm{refold}_i(M_i^{k+1} - \frac{1}{\mu_i}Q_i^k)}{1 + \Sigma_{i=1}^h\mu_i} \tag{13}$$

For term $\mathcal{E}^{k+1}$:

$$\arg\min_{\mathcal{E}} \frac{1}{2}\|\mathcal{P}-\mathcal{L}^{k+1}-\mathcal{E}\|_F^2 + \beta\|\mathcal{E}\|^p_{p,p}. \tag{14}$$

Therefore the element of $\mathcal{E}^{k+1}$ in position (i,j,k) is $GST((\mathcal{P} - \mathcal{L}^{k+1})_{ijk}, \beta, p, J)$, where $(\mathcal{P} - \mathcal{L}^{k+1})_{ijk}$ is the element of $\mathcal{P} - \mathcal{L}^{k+1}$ in position (i,j,k).

III. THE ALGORITHM FOR IMAGE DENOISING

Image denoising aims to reconstruct the original image $\mathcal{L} \in \mathbb{R}^{m\times n\times d}$ from its noisy observation $\mathcal{P} = \mathcal{L} + \mathcal{N} + \mathcal{E}$, where $\mathcal{N}$ and $\mathcal{E}$ are assumed as Gaussian white noise with zero mean and impulse noise, respectively. In this section, the proposed model (6) be applied to image denoising.

Algorithm 2 Image Denoising by Soving (6).

Input: Noisy image $\mathcal{P}$, C, $\sigma_n^{(0)} = \sigma_n$, $\hat{\mathcal{L}}^{(0)} = C\mathcal{P}$ and $\hat{\mathcal{P}}^{(0)} = C\mathcal{P}$
Output: Denoised image $\hat{\mathcal{L}}^{(T)}$
for $t = 1 : T$ **do**
  Iterative regularization
  $\hat{\mathcal{P}}^{(t)} = \hat{\mathcal{L}}^{(t-1)} + \alpha_0(\hat{\mathcal{P}}^{(0)} - \hat{\mathcal{L}}^{(t-1)} - \hat{\mathcal{E}}^{(t-1)})$
  Estimate local noise level
  $\sigma_n^{(t)} = \lambda_0\sqrt{|(\sigma_n^{(0)})^2 - \frac{1}{mnd}\|\hat{\mathcal{P}}^{(t)} - \hat{\mathcal{L}}^{(t-1)} - \hat{\mathcal{E}}^{(t-1)}\|_F^2|}$
  for *each patch* $\mathcal{P}_s$ *in* $\hat{\mathcal{P}}^{(t)}$ **do**
    Find similar patches of $\mathcal{P}_s$ to form tensor $\hat{\mathcal{P}}_s$ from $\hat{\mathcal{P}}^{(t)}$
    Determine weight vector $\mathbf{w}_i^{(t)}$ via Eq.(16)
    Obtain tensor $\hat{\mathcal{L}}_s$ and $\hat{\mathcal{E}}_s$ via Eq.(15)
  end
  Aggregate $\hat{\mathcal{L}}_s$ to form the denoised image $\hat{\mathcal{L}}^{(t)}$
end
Return: The final denoised image $C^{-1}\hat{\mathcal{L}}^{(T)}$

The image denoising algorithm consists of four basic steps: preprocessing (only for color images), patch grouping [8], low-rank tensor recovery, and aggregation. The detail of each step is described in the following parts.

For color image denoising, the RGB channel space is firstly transformed to the YC_bC_r channel space and C represent the transform operator. For grayscale image denoising, C is identity matrix.

Since patch grouping results will be seriously degraded by the impulse noise when $\mathcal{E} \neq 0$, the random-valued impulse noise need to be firstly detected by the adaptive center-weighted median filter (ACWMF) as in [29]. To further improve the effect of algorithm, a characteristic matrix is defined to record the position of the impulse noise obtained by ACWMF. Since ACWMF is impossible to detect accurately all the positions of the random-valued impulse noise. Here, we define the characteristic matrix with 0.3 and 0.7 (instead of 0 and 1) to weight the impulse noise position and non-impulse noise position, and this matrix can be used to weight the term $\|\cdot\|_{p,p}^p$ in the optimization process.

First, Algorithm 2 searches for K nonlocal similar patches of the given patch across the image utilizing block matching [8]. Next, those similar patches are stacked into a 3rd-order tensor $\hat{\mathcal{P}}_s$ which satisfies $\hat{\mathcal{P}}_s = \mathcal{L}_s^* + \mathcal{E}_s^* + \mathcal{N}_s^*$, where $\mathcal{L}_s^*$, $\mathcal{E}_s^*$ and $\mathcal{N}_s^*$ are the patch tensors of original image, impulse noise and Gaussian noise, respectively. Then, the estimations of $\mathcal{L}_s^*$ and $\mathcal{E}_s^*$, $\hat{\mathcal{L}}_s$ and $\hat{\mathcal{E}}_s$, are obtained by the following optimization problem:

$$(\hat{\mathcal{L}}_s, \hat{\mathcal{E}}_s) = \arg\min_{\mathcal{L}_s,\mathcal{E}_s} \frac{1}{2}\|\hat{\mathcal{P}}_s - \mathcal{L}_s - \mathcal{E}_s\|_F^2 + \alpha\|\mathcal{L}_s\|_{\mathbf{w}^{(t)},S_p}^p + \beta\|\mathcal{E}_s\|_{p,p}^p, \quad (15)$$

FIGURE 1. Testing image dataset.

where t is the number of iteration, $\|.\|_F^2$ and $\|.\|_{p,p}^p$ correspond to zero mean Gaussian noise and impulse noise respectively. If we set $\beta \to \infty$, the above model reduces to the original low-rank recovery model [30][1] (which is called weighted tensor Schatten p-norm minimization model, or simply WTSN for short.) defined as follows :

$$\hat{\mathcal{L}}_s = \arg\min_{\mathcal{L}_s} \frac{1}{2}\|\hat{\mathcal{P}}_s - \mathcal{L}_s\|_F^2 + \alpha\|\mathcal{L}_s\|_{\mathbf{w}^{(t)},S_p}^p.$$

Thus model (15) can deal with zero mean Gaussian noise, impulse noise and any other noise that can be approximated by mixing these two kinds of noise. The weighting technique proposed in [21] is adopted for (15). The j-th component of weight vector $\mathbf{w}_i^{(t)}$ is determined as

$$(\mathbf{w}_i)_j^{(t)} = (\sigma_n^{(t)})^2 c\sqrt{K}/((\delta_j^{(t)}(\hat{\mathcal{L}}_{s,(i)}))^{\frac{1}{p}} + \varepsilon), \quad (16)$$

where K is the number of similar patches, c is a positive constant, $\varepsilon = 10^{-16}$ is added to avoid dividing by zero and $\sigma_n^{(t)}$ is the estimation of standard deviation of Gaussian noise in the iteration t. $\hat{\mathcal{L}}_{s,(i)}$ is unfolding matrix of tensor $\hat{\mathcal{L}}_s$ on the i-th mode. Since $\delta_j(\hat{\mathcal{L}}_{s,(i)})$, the j-th singular value of matrix $\hat{\mathcal{L}}_{s,(i)}$, is unavailable before $\hat{\mathcal{L}}_s$ is estimated, it can be initialized by

$$\delta_j^{(t)}(\hat{\mathcal{L}}_{s,(i)}) = \sqrt{\max\{\sigma_j^2(\hat{\mathcal{P}}_{s,(i)}^{(t)} + \frac{1}{\mu_i}Q_i) - K(\sigma_n^{(t)})^2, 0\}}. \quad (17)$$

The denoised image $\hat{\mathcal{L}}^{(t)}$ can be reconstructed by aggregating all the denoised patches together. Algorithm 2 summarizes the whole denoising process, and the iterative regularization scheme mentioned in [11] is adopted in it.

$$\hat{\mathcal{P}}^{(t)} = \hat{\mathcal{L}}^{(t-1)} + \alpha_0(\hat{\mathcal{P}}^{(0)} - \hat{\mathcal{L}}^{(t-1)} - \hat{\mathcal{E}}^{(t-1)}), \quad (18)$$

where α_0 is a relaxation.

[1]Reference [27] is our previous work published as a conference paper.

(a) (b) (c) (d)

FIGURE 2. Denoising results on image"house" by WTSTP and SAIST, noise level $\sigma_n = 30$. (a) Noised image. (b) Original image. (c) Denoised image by WTSTP. (d) Denoised image by SAIST.

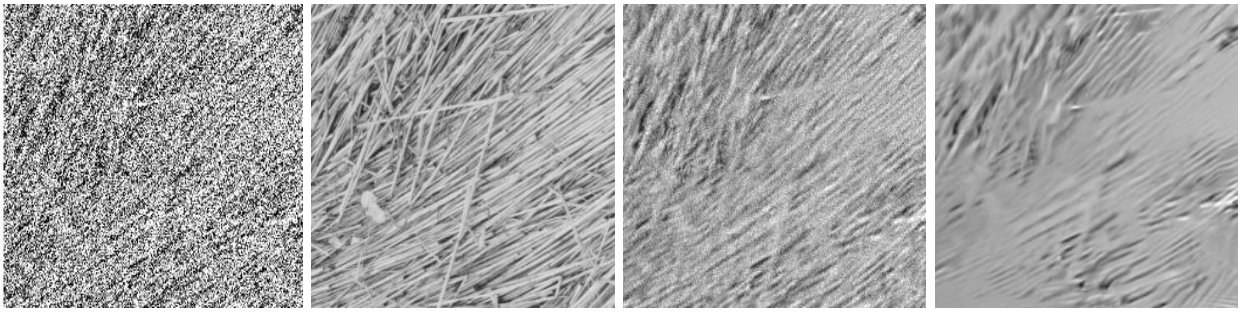

(a) (b) (c) (d)

FIGURE 3. Denoising results on image "straw" by WTSTP and SAIST, noise level $\sigma_n = 100$. (a) Noised image. (b) Original image. (c) Denoised image by WTSTP. (d) Denoised image by SAIST.

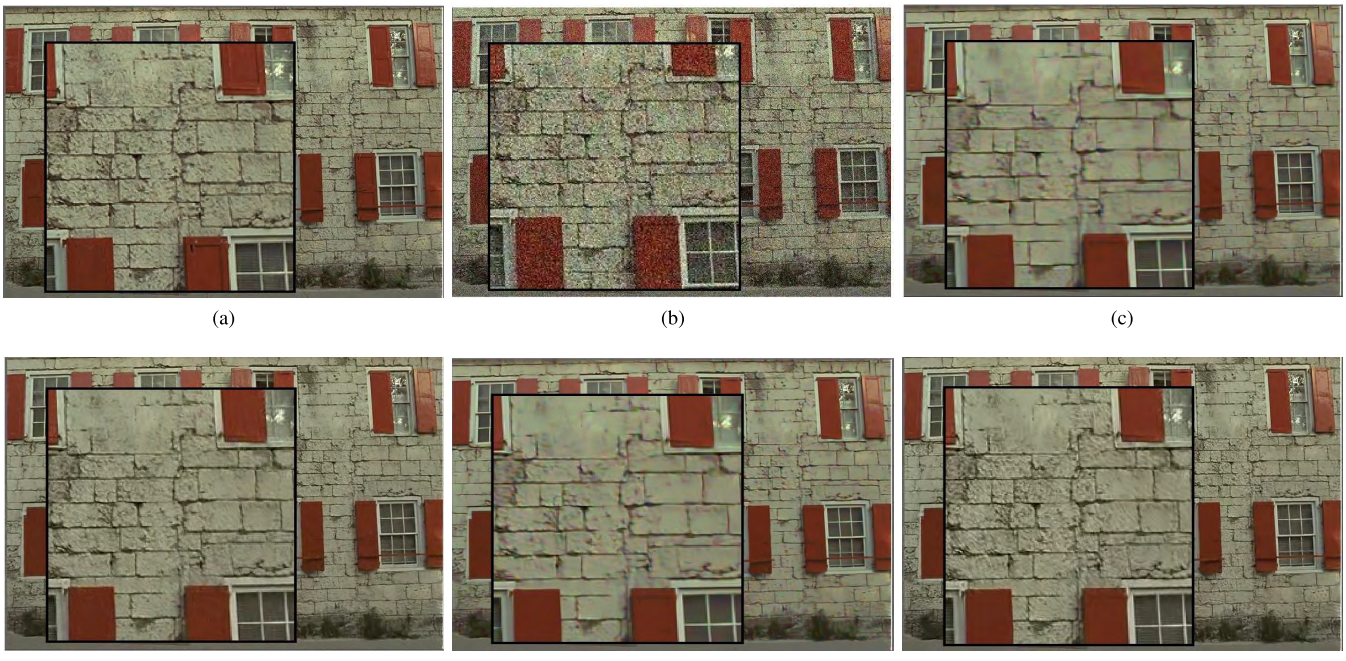

(a) (b) (c)

(d) (e) (f)

FIGURE 4. Denoised results on "Kodak image1", $\sigma_n = 30$. (a) Original. (b) Noisy. (c) BM3D. (d) WTNN. (e) WSNM. (f) WTSTP.

IV. EXPERIMENTAL RESULTS AND ANALYSIS

In this section, three different experiments are carried out to prove the effectiveness of the proposed image denoising method.

A. REMOVING GAUSSIAN NOISE IN GRAYSCALE IMAGE

The proposed denoising method is compared with a series of state-of-the-art denoising methods, including Block-matching 3D Filtering [8] (BM3D), Patch-based

TABLE 1. Denoising results (PSNR) by different methods.

$\sigma_n = 20$							$\sigma_n = 30$					
Image	**BM3D**	**PBNO**	**EPLL**	**GID**	**SAIST**	**WTSTP**	**BM3D**	**PBNO**	**EPLL**	**GID**	**SAIST**	**WTSTP**
House	33.77	33.58	32.98	32.81	33.75	**33.78**	32.08	31.92	31.22	30.35	31.39	**32.14**
Monarch	30.35	29.55	30.48	29.65	30.76	**30.90**	28.36	27.85	28.35	27.60	28.03	**28.46**
Airplane	32.53	32.06	32.41	31.48	32.39	**32.63**	27.56	30.21	30.41	29.47	29.35	**30.55**
Barbara	31.77	31.06	29.76	30.21	**32.10**	31.90	29.81	29.50	27.56	27.95	**30.04**	29.68
Boat	**30.88**	30.39	30.66	29.53	30.84	30.82	**29.11**	28.81	28.89	27.66	28.83	28.77
Bridge	27.27	26.70	**27.49**	26.49	27.31	27.42	25.46	25.22	**25.68**	24.78	25.43	25.47
Couple	**30.76**	30.22	30.54	29.28	30.66	30.56	**28.86**	28.58	28.61	27.15	28.58	28.46
F.print	28.80	27.76	28.28	27.95	28.99	**29.12**	26.82	26.35	26.18	26.00	26.82	**26.97**
Hill	**30.72**	30.32	30.49	29.59	30.58	30.67	**29.15**	28.95	28.90	27.75	28.94	28.86
Lena	33.05	32.75	32.61	31.74	**33.08**	32.92	**31.26**	31.16	30.78	29.83	30.77	31.06
Man	30.59	30.15	30.63	29.59	30.54	**30.65**	**28.86**	28.65	28.82	27.82	28.68	28.61
Straw	27.07	25.86	26.92	26.63	27.23	**27.62**	24.94	24.70	24.74	24.59	24.74	**25.17**
Average	30.63	30.03	30.27	29.58	30.69	**30.75**	28.52	28.49	28.35	27.58	28.47	**28.68**
$\sigma_n = 50$							$\sigma_n = 60$					
Image	**BM3D**	**PBNO**	**EPLL**	**GID**	**SAIST**	**WTSTP**	**BM3D**	**PBNO**	**EPLL**	**GID**	**SAIST**	**WTSTP**
House	29.69	29.44	28.76	27.62	**29.99**	29.77	28.73	28.62	27.84	26.66	28.88	**29.08**
Monarch	25.81	25.53	25.77	24.97	**26.09**	26.07	24.97	24.64	24.85	24.15	24.94	**25.20**
Airplane	25.10	27.77	27.88	26.91	28.25	**28.26**	27.32	26.98	26.97	25.82	26.64	**27.35**
Barbara	27.22	26.95	24.82	25.17	27.49	**27.50**	26.28	26.08	23.87	24.19	**26.40**	**26.40**
Boat	**26.78**	26.67	26.65	25.59	26.63	26.72	**26.02**	25.94	25.84	24.68	25.52	25.71
Bridge	23.57	23.49	**23.69**	22.88	23.49	23.60	23.02	22.90	**23.08**	22.19	22.85	22.83
Couple	**26.46**	26.30	26.23	24.64	26.29	26.29	**25.66**	25.43	25.40	24.01	24.98	25.41
F.print	24.52	24.29	23.59	23.09	24.54	**24.72**	23.75	23.57	22.65	21.90	23.71	**23.86**
Hill	**27.19**	27.02	26.95	25.93	27.04	27.08	**26.52**	26.27	26.27	25.32	**26.39**	26.30
Lena	**29.05**	28.81	28.42	27.69	29.01	28.98	**28.27**	27.92	27.59	26.91	28.00	28.10
Man	**26.80**	26.72	26.72	25.83	26.67	26.70	**26.13**	26.00	26.00	25.14	25.78	25.92
Straw	22.40	22.81	22.00	21.98	22.65	**22.93**	21.63	22.01	21.06	20.93	**22.13**	22.12
Average	26.22	26.32	25.96	25.19	26.51	**26.55**	**25.69**	25.53	25.12	24.33	25.52	**25.69**
$\sigma_n = 75$							$\sigma_n = 100$					
Image	**BM3D**	**PBNO**	**EPLL**	**GID**	**SAIST**	**WTSTP**	**BM3D**	**PBNO**	**EPLL**	**GID**	**SAIST**	**WTSTP**
House	27.50	27.15	26.68	25.16	**27.90**	27.85	25.87	25.42	25.19	23.59	**26.45**	26.34
Monarch	23.90	23.62	23.71	22.77	23.95	**24.01**	22.51	22.19	22.23	20.83	**22.63**	22.49
Airplane	**26.31**	25.83	25.83	24.69	25.82	26.28	22.11	24.31	24.35	23.28	24.55	**24.90**
Barbara	25.12	24.94	22.94	23.06	25.35	**25.37**	23.62	23.42	22.14	21.76	23.98	**24.03**
Boat	**25.14**	24.85	24.88	23.81	24.80	24.98	**23.97**	23.62	23.71	22.74	23.67	23.79
Bridge	**22.40**	22.26	22.39	21.52	22.07	22.26	**21.60**	21.42	21.58	20.74	21.21	21.47
Couple	**24.70**	24.51	24.44	23.27	24.17	24.43	23.51	23.28	23.32	22.38	23.01	**23.79**
F.print	22.83	22.67	21.46	20.43	22.72	**22.94**	21.61	21.50	19.84	18.74	21.51	**21.74**
Hill	**25.67**	25.45	25.45	24.62	25.50	25.52	**24.58**	24.33	24.42	23.79	24.29	24.53
Lena	**27.25**	27.00	26.57	25.96	26.97	27.17	**25.95**	25.60	25.30	24.64	25.81	25.84
Man	**25.31**	25.11	25.14	24.38	25.06	25.10	**24.22**	23.98	24.07	23.33	23.98	24.06
Straw	20.72	21.04	20.07	19.55	21.08	**21.13**	19.58	19.86	19.01	18.41	19.54	**20.08**
Average	24.74	24.54	24.13	23.27	24.62	**24.75**	23.26	23.24	22.93	22.02	23.39	**23.59**

Near-optimal Image Denoising [31] (PBNO), Expected Patch Log Likelihood for Image Denoising [32] (EPLL) Global Image Denoising [33] (GID) and Spatially Adaptive Iterative Singular-value Thresholding [3] (SAIST).

The implementation details of this part are set as follows: all these methods are tested on 12 images (see Fig. 1). Gaussian noise with variance σ_n^2 is added to these images to get the noised observations, where $\sigma_n = \{20, 30, 50, 60, 75, 100\}$. The size of searching window for similar patches is 30×30. According to noise level, patch size and iteration number are set. For heavy noise, more iterations and bigger patches are chosen. More exactly, the iteration number T is set to $T = \{8, 8, 12, 14\}$, the size of each patch is set to be $\{6 \times 6, 7\times7, 8\times8, 9\times9\}$ and $p = \{0.95, 0.8, 0.7, 0.5\}$ for $\sigma_n \leq 20$, $20 < \sigma_n \leq 30$, $30 < \sigma_n \leq 60$ and $60 < \sigma_n \leq 100$, respectively.

Table 1 shows the peak-signal-to-noise-ratio (PSNR) results by different methods. On each noise level, the highest PSNR result for each image is highlighted in bold. An overall impression observed from the table is that WTSTP achieves at least comparable denoising performance to other five methods, and it outperforms other methods by 0.15dB on average in most cases. The reason is that both local and nonlocal information within the image can be effectively combined for image denoising.

The "house" image (see Fig. 2) and the "straw" image (see Fig. 3) are picked up to show the denoised results in terms of visual quality. Here, our method is compared with SAIST. Since compared with other methods, denoising results of SAIST are the best. It is clear that our method retains much more structures information and detail within the image than SAIST. In a word, our method presents strong denoising

TABLE 2. Color image denoising results (PSNR) by different methods.

$\sigma = 5$					$\sigma = 10$				
	BM3D	WTNN	WSNM	WTSTP		BM3D	WTNN	WSNM	WTSTP
House	38.66	**39.02**	38.86	39.01	House	35.57	36.10	35.74	**36.14**
Peppers	36.92	37.05	**37.10**	37.03	Peppers	33.81	33.92	**33.98**	33.94
Lena	37.58	**37.98**	37.74	37.96	Lena	34.80	35.21	34.90	**35.23**
Baboon	35.13	**35.39**	35.28	**35.39**	Baboon	30.25	30.86	30.53	**30.87**
F16	38.94	**39.76**	39.11	39.75	F16	35.68	**36.56**	35.90	**36.56**
Kodak image1	36.15	**39.30**	36.35	**39.30**	Kodak image1	31.62	34.66	31.93	**34.67**
Kodak image2	38.26	**40.45**	38.65	**40.45**	Kodak image2	34.75	36.61	35.11	**36.64**
Kodak image3	40.59	**42.42**	40.91	42.41	Kodak image3	37.01	38.92	37.32	**38.99**
Kodak image12	39.14	**41.36**	39.39	41.35	Kodak image12	35.80	37.84	36.01	**37.89**
Average	37.93	**39.19**	38.15	39.18	Average	34.37	35.63	34.60	**35.66**
$\sigma = 20$					$\sigma = 30$				
	BM3D	WTNN	WSNM	WTSTP		BM3D	WTNN	WSNM	WTSTP
House	33.00	**33.38**	33.15	33.36	House	31.49	31.31	31.91	**31.96**
Peppers	31.62	31.66	31.62	**31.70**	Peppers	30.33	30.02	30.43	**30.45**
Lena	32.29	32.76	32.34	**32.82**	Lena	30.73	30.71	30.89	**31.39**
Baboon	26.16	**27.01**	26.48	26.96	Baboon	24.14	**25.26**	24.42	25.18
F16	32.54	**33.46**	32.78	**33.46**	F16	30.72	30.97	30.96	**31.65**
Kodak image1	27.81	30.54	28.15	**30.55**	Kodak image1	26.09	28.15	26.33	**28.48**
Kodak image2	32.03	33.10	32.12	**33.12**	Kodak image2	30.68	30.62	30.82	**31.35**
Kodak image3	33.59	35.43	33.81	**35.52**	Kodak image3	31.84	32.25	32.02	**33.60**
Kodak image12	32.93	34.45	32.98	**34.47**	Kodak image12	31.40	31.68	31.51	**32.60**
Average	31.33	32.42	31.49	**32.44**	Average	29.71	30.11	29.92	**30.74**

TABLE 3. Results (PSNR) on Lena and Barbara by different methods in the case of Gaussian-impulse mixed noise.

		Lena			Barbara		
σ	r(%)	Cai'work	Xiao'work	WTSTP	Cai'work	Xiao'work	WTSTP
5	10	32.77	**34.98**	34.45	25.33	30.48	**33.02**
	20	31.78	**33.64**	33.27	24.72	27.76	**30.96**
	30	30.69	**32.04**	31.63	24.10	25.92	**29.54**
10	10	30.80	32.75	**32.87**	24.46	28.42	**31.21**
	20	30.02	31.66	**31.70**	23.99	26.59	**30.19**
	30	29.08	**30.42**	30.22	23.66	25.34	**28.46**
15	10	29.13	30.85	**31.49**	23.80	27.31	**30.07**
	20	28.59	29.98	**30.21**	23.60	25.69	**28.60**
	30	27.96	29.11	**29.16**	23.27	24.55	**27.24**

ability in both visual perception quality and quantitative measure.

B. REMOVING GAUSSIAN NOISE IN COLOR IMAGE

In this part, our method is compared with three state-of-the-art denoising methods for color image denoising: Block-matching 3D Filtering (BM3D) [8], Weighted Tensor Nuclear Norm Minimization (WTNN) [9] and Weighted Schatten p-norm Minimization (WSNM) [21]. The testing image set contains House, Lena, Pappers, F16, Baboon, the $1-3^{th}$ and 12^{th} images from the Kadak PhotoCD. In this experiment, additive white Gaussian noise with standard deviation $\sigma_n = \{5, 10, 20, 30\}$ is added to those images to obtain the noised images, and we set the iteration number as $T = \{5, 3, 8, 10\}$, and $p = \{0.97, 0.9, 0.9, 0.9\}$ for $\sigma_n \leq 5$, $5 < \sigma_n \leq 10$, $10 < \sigma_n \leq 20$ and $20 < \sigma_n \leq 30$, respectively.

Similarly, the PSNR value and visual quality are used to evaluate the effectiveness of our method, the PSNR value results are presented in Table 2 and the highest PSNR value is highlighted in each cell. As shown in the Table 2 and Fig.4, our method obviously outperforms the other two methods, and the reasons are analyzed as follows. (1) Our method v.s. WTNN: the weighted tensor schatten p-norm requires the weaker incoherence conditions than weighted tensor nuclear norm minimization, and thus is more robust against noise and outliers. (2) Our method v.s. BM3D and WSNM: BM3D and WSNM handle the image channels separately in the process of color image, while our method handles the image channels in an unified framework, and the correlation information among the image channels is effectively used.

C. ZERO MEAN GAUSSIAN-IMPULSE MIXED NOISE

In this part, the proposed work is compared with Cai's work [34] and Xiao's work [29] in case of zero mean Gaussian-impulse mixed noise, where the testing data include Lena and Barbara. To have a fair comparison, the noise level is set the same as in [29]: zero mean Gaussian noise with standard deviations $\sigma = \{5, 10, 15\}$ and random-valued impulse noise with density level $r = \{10\%, 20\%, 30\%\}$.

The denoising results obtained by different methods are shown in Table 3,[2] from which we can find that the denoising performance has greatly promoted in most cases. The reasons are as follows: (1) both local and nonlocal information within the image can be effectively combined for image denoising.

[2]Since there is no code of the compared methods in the experiment, our work is directly compared with the experimental results in the paper of those under the same parameter settings, and thus only quantitative analysis has been given.

(2) WTSTP yields a desired sparse solution, and thus is more robust against noise and outliers. (3) in our work, the impulse noise detection results obtained by ACWMF are only provided as a prior for Algorithm 2, and the sparse error term in our models can effectively compensate it and find the impulse noise which is not accurately detected by ACWMF.

V. CONCLUSIONS

In this paper, we have proposed a new low-rank tensor recovery model: joint weighted tensor Schatten p-norm and tensor l_p-norm minimization (WTSTP) for image denoising. WTSTP has two major merits: On the one hand, it treats the image patches as tensor instead of vector, and thus makes full use of the structure information and the relation of different channels within the image which can improve the denoising performance; On the other hand, it adopts l_p-norm and Schatten p-norm which is robust against noise and outliers and ensures a more accurate low-rank recovery. Meanwhile, it can deal with any noise that can be approximated by mixing zero mean Gaussian noise and impulse noise. In the part of experiment, the proposed algorithm was applied to grayscale image denoising and color image denoising, and the experimental results demonstrated the validity of our work. In the future, we expect WTSTP will be applied in other fields except for image denoising.

ACKNOWLEDGEMENTS

The authors would like to thank the anonymous reviewers for many the helpful comments.

REFERENCES

[1] J. Portilla, V. Strela, M. J. Wainwright, and E. P. Simoncelli, "Image denoising using scale mixtures of Gaussians in the wavelet domain," *IEEE Trans. Image Process.*, vol. 12, no. 11, pp. 1338–1351, Nov. 2003.
[2] A. L. da Cunha, J. Zhou, and M. N. Do, "The nonsubsampled contourlet transform: Theory, design, and applications," *IEEE Trans. Image Process.*, vol. 15, no. 10, pp. 3089–3101, Oct. 2006.
[3] W. Dong, G. Shi, and X. Li, "Nonlocal image restoration with bilateral variance estimation: A low-rank approach," *IEEE Trans. Image Process.*, vol. 22, no. 2, pp. 700–711, Feb. 2013.
[4] S. Gu, L. Zhang, W. Zuo, and X. Feng, "Weighted nuclear norm minimization with application to image denoising," in *Proc. IEEE Conf. Comput. Vis. Pattern Recognit.*, Jun. 2014, pp. 2862–2869.
[5] A. Buades, B. Coll, and J.-M. Morel, "A non-local algorithm for image denoising," in *Proc. IEEE Comput. Soc. Conf. Comput. Vis. Pattern Recognit.*, Jun. 2005, pp. 60–65.
[6] V. Papyan and M. Elad, "Multi-scale patch-based image restoration," *IEEE Trans. Image Process.*, vol. 25, no. 1, pp. 249–261, Jan. 2016.
[7] M. Nejati, S. Samavi, H. Derksen, and K. Najarian, "Denoising by low-rank and sparse representations," *J. Vis. Commun. Image Represent.*, vol. 36, no. C, pp. 28–39, Apr. 2016.
[8] K. Dabov, A. Foi, V. Katkovnik, and K. Egiazarian, "Image denoising by sparse 3-D transform-domain collaborative filtering," *IEEE Trans. Image Process.*, vol. 16, no. 8, pp. 2080–2095, Aug. 2007.
[9] K. Hosono, S. Ono, and T. Miyata, "Weighted tensor nuclear norm minimization for color image denoising," in *Proc. IEEE Int. Conf. Image Process.*, Sep. 2016, pp. 3081–3085.
[10] A. Eriksson and A. van den Hengel, "Efficient computation of robust low-rank matrix approximations in the presence of missing data using the L_1 norm," in *Proc. IEEE Conf. Comput. Vis. Pattern Recognit.*, Jun. 2010, pp. 771–778.
[11] A. M. Buchanan and A. W. Fitzgibbon, "Damped Newton algorithms for matrix factorization with missing data," in *Proc. IEEE Conf. Comput. Vis. Pattern Recognit.*, Jun. 2005, pp. 316–322.
[12] M. Partridge and M. Jabri, "Robust principal component analysis," in *Proc. IEEE Signal Process. Soc. Workshop*, Dec. 2000, pp. 289–298.
[13] M. Fazel, H. Hindi, and S. P. Boyd, "A rank minimization heuristic with application to minimum order system approximation," in *Proc. Amer. Control Conf.*, vol. 6, Jun. 2001, pp. 4734–4739.
[14] F. Nie, H. Huang, and C. Ding, "Low-rank matrix recovery via efficient schatten p-norm minimization," in *Proc. AAAI Conf. Artif. Intell.*, 2012, pp. 655–661.
[15] K. Mohan and M. Fazel, "Iterative reweighted algorithms for matrix rank minimization," *J. Mach. Learn. Res.*, vol. 13, no. 1, pp. 3441–3473, 2012.
[16] E. J. Candès, X. Li, Y. Ma, and J. Wright, "Robust principal component analysis?" *J. ACM*, vol. 58, no. 3, p. 11, 2011.
[17] E. J. Candes and B. Recht, "Exact low-rank matrix completion via convex optimization," in *Proc. 46th Annu. Allerton Conf. Commun., Control, Comput.*, Sep. 2008, pp. 806–812.
[18] J.-F. Cai, E. J. Candès, and Z. Shen, "A singular value thresholding algorithm for matrix completion," *SIAM J. Optim.*, vol. 20, no. 4, pp. 1956–1982, 2008.
[19] R. Chartrand, "Exact reconstruction of sparse signals via nonconvex minimization," *IEEE Signal Process. Lett.*, vol. 14, no. 10, pp. 707–710, Oct. 2007.
[20] L. Liu, W. Huang, and D.-R. Chen, "Exact minimum rank approximation via Schatten p-norm minimization," *J. Comput. Appl. Math.*, vol. 267, pp. 218–227, Sep. 2014.
[21] Y. Xie, S. Gu, Y. Liu, W. Zuo, W. Zhang, and L. Zhang, "Weighted schatten p-norm minimization for image denoising and background subtraction," *IEEE Trans. Image Process.*, vol. 25, no. 10, pp. 4842–4857, Oct. 2016.
[22] J. Liu, P. Musialski, P. Wonka, and J. Ye, "Tensor completion for estimating missing values in visual data.," *IEEE Trans. Pattern Anal. Mach. Intell.*, vol. 35, no. 1, pp. 208–220, Jan. 2013.
[23] M. Signoretto, R. Van de Plas, B. De Moor, and J. A. K. Suykens, "Tensor versus matrix completion: A comparison with application to spectral data," *IEEE Signal Process. Lett.*, vol. 18, no. 7, pp. 403–406, Jul. 2011.
[24] T. G. Kolda and B. W. Bader, "Tensor decompositions and applications," *SIAM Review*, vol. 51, no. 3, pp. 455–500, 2009.
[25] B. Huang, C. Mu, D. Goldfarb, and J. Wright. (2014). *Provable Low-Rank Tensor Recovery*. [Online]. Available: http://www.optimization-online.org/DB_HTML/2014/02/4252.html
[26] C. Lu, J. Feng, Y. Chen, W. Liu, Z. Lin, and S. Yan, "Tensor robust principal component analysis: Exact recovery of corrupted low-rank tensors via convex optimization." in *Proc. IEEE Conf. Comput. Vis. Pattern Recognit.*, Jun. 2017, pp. 5249–5257.
[27] Z. Lin, M. Chen, and Y. Ma. (Sep. 2010). "The augmented Lagrange multiplier method for exact recovery of corrupted low-rank matrices," p. 9. [Online]. Available: https://arxiv.org/abs/1009.5055
[28] W. Zuo, D. Meng, L. Zhang, X. Feng, and D. Zhang, "A generalized iterated shrinkage algorithm for non-convex sparse coding," in *Proc. IEEE Int. Conf. Comput. Vis.*, Dec. 2013, pp. 217–224.
[29] Y. Xiao, T. Zeng, J. Yu, and M. Ng, "Restoration of images corrupted by mixed Gaussian-impulse noise via $\mathcal{L}_1 - \mathcal{L}_0$ minimization," *Pattern Recognit.*, vol. 44, no. 8, pp. 1708–1720, 2011.
[30] Y. Yan, X. Zhang, J. Zheng, and L. Zhao, "Weighted tensor schatten p-norm minimization for image denoising," in *Proc. Chin. Intell. Syst. Conf.*, 2019, pp. 163–172.
[31] P. Chatterjee and P. Milanfar, "Patch-based near-optimal image denoising," *IEEE Trans. Image Process.*, vol. 21, no. 4, pp. 1635–1649, Apr. 2012.
[32] D. Zoran and Y. Weiss, "From learning models of natural image patches to whole image restoration," in *Proc. IEEE Int. Conf. Comput. Vis.*, Nov. 2011, pp. 479–486.
[33] H. Talebi and P. Milanfar, "Global image denoising," *IEEE Trans. Image Process.*, vol. 23, no. 2, pp. 755–768, Feb. 2014.
[34] J. F. Cai, R. Chan, and M. Nikolova, "Two-phase methods for deblurring images corrupted by impulse plus Gaussian noise," *Inverse Problem Imag.*, vol. 2, no. 2, pp. 187–204, 2008.

Authors' photographs and biographies not available at the time of publication.